Steel and Composite Structures, *Vol. 33, No. 2* (*2019*) *195-208*
DOI: https://doi.org/10.12989/scs.2019.33.2.195

Vibration analysis of functionally graded graphene platelet-reinforced composite doubly-curved shallow shells on elastic foundations

Mohammed Sobhy*[1,3] and Ashraf M. Zenkour [2,3a]

[1] *Department of Mathematics and Statistics*, *Faculty of Science*, *King Faisal University*, *P.O. Box 400*, *Hofuf 31982*, *Saudi Arabia*
[2] *Department of Mathematics*, *Faculty of Science*, *King Abdulaziz University*, *P.O. Box 80203*, *Jeddah 21589*, *Saudi Arabia*
[3] *Department of Mathematics*, *Faculty of Science*, *Kafrelsheikh University*, *Kafrelsheikh 33516*, *Egypt*

(*Received November 16, 2018, Revised September 10, 2019, Accepted October 4, 2019*)

Abstract. Based on a four-variable shear deformation shell theory, the free vibration analysis of functionally graded graphene platelet-reinforced composite (FGGPRC) doubly-curved shallow shells with different boundary conditions is investigated in this work. The doubly-curved shells are composed of multi nanocomposite layers that are reinforced with graphene platelets. The graphene platelets are uniformly distributed in each individual layer. While, the volume faction of the graphene is graded from layer to other in accordance with a novel distribution law. Based on the suggested distribution law, four types of FGGPRC doubly-curved shells are studied. The present shells are assumed to be rested on elastic foundations. The material properties of each layer are calculated using a micromechanical model. Four equations of motion are deduced utilizing Hamilton's principle and then converted to an eigenvalue problem employing an analytical method. The obtained results are checked by introducing some comparison examples. A detailed parametric investigation is performed to illustrate the influences of the distribution type of volume fraction, shell curvatures, elastic foundation stiffness and boundary conditions on the vibration of FGGPRC doubly-curved shells.

Keywords: doubly-curved nanocomposite shells; functionally graded; graphene platelets; vibration; elastic foundations; four-variable shell theory

1. Introduction

Doubly-curved nanocomposite shells are considered the most common structural elements used in modern industries. A few typical examples of shell constructions contain automobile bodies, pressure vessels, silos, ship hulls, wings, aviation vehicle fuses, rockets, branching and intersecting pipelines, submarine hulls, etc. For this reason, it is important to develop the right models for shell constructions. So far, several studies have been done on the examination of the shells. The free vibration frequencies are considered as the most important item to study the properties of doubly-curved shells.

Many problems related with the modeling and behavior in free vibration of doubly-curved shells have been found in the literature (Chandrashekhara 1989, Qatu and Leissa 1991, Bhimaraddi 1991, Liew and Lim 1996, 1997, Tan 1998, Singh 1999, Hause and Librescu 2007, Monterrubio 2009, Tornabene 2011a, Qatu and Asadi 2012, Mochida *et al*. 2012, Tornabene *et al*. 2013, Ghavanloo and Fazelzadeh 2013, Jiang *et al*. 2013, Arefi 2018, Rezaiee *et al*. 2018, Nasihatgozar *et al*. 2017). Chandrashekhara (1989) has discussed the free vibration characteristics of laminated composite shells using an isoparametric doubly-curved quadrilateral shear flexible element and first-order shear deformation shell theory. Qatu and Leissa (1991) have discussed the free vibrations of cantilevered doubly-curved laminated composite shallow shells. Bhimaraddi (1991) have investigated the free vibration of doubly-curved shallow shells on rectangular planform using 3-D elasticity theory. Liew and Lim (1996, 1997) have investigated the free vibration of thin and thick doubly-curved shallow shells of rectangular and elliptic planforms. Tan (1998) predicted the natural frequencies of shells of revolution with arbitrary shape and general material properties subjected to different boundary conditions. Singh (1999) has presented the free vibration of doubly-curved sandwich shells made of thin outer layers and a relatively thick core. Hause and Librescu (2007) have discussed the modeling and free vibration of doubly-curved anisotropic sandwich panels. The free vibration frequencies of doubly-curved shells and panels using the Rayleigh–Ritz method and 2-D GDQ have been presented in Monterrubio (2009) and Tornabene (2011b). Qatu and Asadi (2012) used thin shell theory to study the vibrations of doubly curved shallow shells. The 2D and 3D free vibration analyses of anisotropic doubly curved shallow shells with general elastic restraints using the superposition-Galerkin and radial basis function methods have been investigated in Refs. (Mochida *et al*. 2012, Tornabene *et al*. 2013, Ghavanloo and Fazelzadeh 2013, Jiang *et al*. 2013).

Graphene has attracted a considerable attention of scientists and engineers to use in many applications because of its extraordinary thermal, mechanical, electrical and chemical properties. Extensive works have been

*Corresponding author, Ph.D.,
E-mail: msobhy@kfu.edu.sa
[a] Ph.D., E-mail: zenkour@kau.edu.sa

ISSN: 1229-9367 (Print), 1598-6233 (Online)

implemented to examine the properties and responses of graphene nanoplates (see, e.g., Refs. (Ni *et al*. 2010, Mahdavi *et al*. 2012, Karami *et al*. 2018a, Voloshina and Dedkov 2014, Hosseini and Zhang 2018, Sobhy and Zenkour 2018, Zenkour and Sobhy 2018, Karami *et al*. 2019)). Recently, graphene platelets (nanosheets) have been utilized as a reinforcement to the polymer materials. The experimental investigations reveal that by adding small amount of graphene platelets to the polymer matrix, high performance graphene nanocomposites are developed. Moreover, the material properties are noticeable improved (70\% in the tensile strength (Fang *et al*. 2009), 57.2\% in Young's modulus (Fang *et al*. 2009), 150\% in tensile strength (Zhao *et al*. 2010), 1000\% in Young's modulus (Zhao *et al*. 2010), 300\% in the flexural bending (Yavari *et al*. 2010), 66\% in the flexural strength (Pathak *et al*. 2016), 72\% in Young's modulus (Pathak *et al*. 2016), 25\% in the shear strength (Pathak *et al*. 2016) and buckling load increased 52\% (Rafiee *et al*. 2009)). Motivated by this regard, number of theoretical works have been introduced in the open literature to investigate the behaviors of the graphene platelets-reinforced nanocomposites such as buckling and postbuckling of FG graphene/epoxy composite plates (Shen *et al*. 2017) and beams (Yang *et al*. 2017a) resting on Pasternak foundation, dynamic instability, buckling and free vibration of FGGPRC nanobeams (Wu *et al*. 2017b), bending of FGGPRC circular and annular plates (Yang *et al*. 2017b), free and forced vibrations and dynamic deflection of FGGPRC plates (Song *et al*. 2017), thermal buckling of FGGPRC plates (Wu *et al*. 2017a), nonlinear buckling of FGGPRC shells (Sahmani and Aghdam 2017) and dynamic and instability analyses of FGGPRC sandwich curved nanobeams (Sobhy and Abazid 2019). In addition, Karami *et al*. (2018b) illustrated the size-dependent static, stability and dynamic response of functionally graded carbon nanotube reinforced composite plates resting on elastic foundations.

Plates resting on elastic foundations are important in structural engineering and have wide engineering applications. Such models can be found in several types of industrial applications such as raft foundations, swimming pools, storage tanks and in most civil engineering constructions. A simple and commonly employed one is Winkler model where it is assumed that the foundation soil consists of linear elastic springs and each spring is independent of the others. However, because of the discontinuity of the soil, this model does not have enough accuracy. To overcome this problem, more complicated and realistic foundation models have been developed such as Pasternak's model (Pasternak 1954) and Vlasov model (Vlasov and Leontev 1966). Several papers have been published in the literature studying the effects of the elastic foundations on the behaviour of various structures (see, e.g., Zenkour *et al*. 2010a, b, Shahsavari *et al*. 2018a, b, c, Abazid *et al*. 2018, Sobhy and Zenkour 2019a, Sobhy 2019).

Recently, there exist some literatures on the free vibration of functionally graded doubly-curved composite shells, and their numerical results are very useful for the practical applications (Pradyumna and Bandyopadhyay 2008, Matsunaga 2008, Chorfi and Houmat 2010, Fadaee *et al*. 2016, Pouresmaeeli and Fazelzadeh 2016, Li *et al*. 2017). Several of foundation models have been developed to study the vibration behavior of doubly-curved composite shells. Most of these researches have dealt with the static and dynamic analyses of FGM doubly curved panels resting on elastic foundation (Tornabene 2011b, Kiani *et al*. 2012, Duc 2013, Bich *et al*. 2014, Duc *et al*. 2017, Najafi *et al*. 2017). However, no papers have been introduced in the literature to investigate the vibrational analysis of functionally graded graphene platelet-reinforced doubly-curved shallow shells on elastic foundations. Moreover, a refined four-variable shear deformation shell theory is proposed here to analyze the present problem.

This article is devoted to illustrate the free vibration of FGGPRC doubly-curved shallow shells with different boundary conditions resting on an elastic substrate. The doubly-curved shell is composed of multi nanocomposite sheets. Each sheet is made of isotropic epoxy matrix reinforced with randomly oriented graphene platelets that are uniformly distributed through the sheet. The volume fraction of the graphene may be the same in all layers or functionally graded along the thickness direction according to a layerwise distribution law. Four types of FGGPRC doubly-curved shallow shells are considered. In accordance with a four-variable shear deformation shell theory, the equations of motion are obtained and then solved analytically under various boundary conditions. The obtained results are compared well with the published ones. In addition, influences of the different parameters such as the power law index, shallowness ratios, aspect ratio, side-to-thickness ratio, foundation stiffness, weight fraction of graphene, boundary conditions and shell types on the vibration of the FGGPRC doubly-curved shallow shells.

2. Functionally graded doubly-curved multi nanocomposite layers

Consider a doubly-curved shell composed of multi nanocomposite homogeneous layers which have the same length a, width b and total thickness h. Each layer is made of mixture of two components, polymer matrix and graphene platelets. The graphene platelets are uniformly dispersed through each layer while its volume fraction changes from layer to other. The curvilinear coordinates (ξ_1, ξ_2, ξ_3) are employed to describe the deformations of the doubly-curved shell (see, Fig. 1). The mid-plane of the panel is defined by $\xi_3 = 0$ and the external surfaces are defined by $\xi_3 = \pm h/2$. The radii of principal curvature of the mid-plane of the shell are given by R_1 and R_2. Several kinds of doubly-curved shells may be considered, namely, circular cylindrical shell ($R_2 = \infty$), spherical shell ($R_1 = R_2$), hyperbolic paraboloidal shell ($R_1 = -R_2$) and other kinds may be developed for different constant values of the curvatures R_1 and R_2.

According to a new law for the distribution of graphene platelets through the thickness of the panel, there are four patterns as shown in Fig. 1. The first is U-GPLs. In this type, the graphene platelet distribution is the same in each

layer. For the second type V-FG, the weight fraction of the graphene platelet increases from the bottom layer to the top one. However, X-FG represents the third type, in which the top and bottom layers are graphene platelet-rich. Whereas, in the fourth type (O-FG), the middle layers are graphene platelet-rich. The volume fractions of the graphene $V_G^{(i)}$ and polymer matrix $V_m^{(i)}$ in ith layer are related as follows

$$V_G^{(i)} + V_m^{(i)} = 1, \tag{1}$$

where the volume fraction of the graphene for the above four patterns is given by

$$V_G^{(i)} = V_{min} + (V_G^* - V_{min})\Gamma^{(i)}, \tag{2}$$

in which V_{min} represents the minimum graphene volume fraction which will be given later, and $\Gamma^{(i)}$ can be given as (Sobhy 2018)

$$\Gamma^{(i)} = \begin{cases} 1, & \text{for } U\text{-GPLs;} \\ \left(\dfrac{i-1}{N-1}\right)^k, & \forall N \in \mathbb{N}, \quad N > 1, \text{ for } V\text{-FG;} \\ \left(\dfrac{|2i-N-1|-1}{N-2}\right)^k, & \forall N \in \mathbb{N}_{\text{even}}, N > 2, \\ & \text{for } X\text{-FG;} \\ \left(\dfrac{|2i-N-1|+1-N}{2-N}\right)^k, & \forall N \in \mathbb{N}_{\text{even}}, N > 2, \\ & \text{for } O\text{-FG,} \end{cases} \tag{3}$$

where N is the number of layers, k is the power law index. Note that, if $k = 0$, one obtains the type of U-GPLs. However, V_G^* is expressed as (Song *et al*. 2017, Feng *et al*. 2017)

$$V_G^* = \frac{\rho_m W_G}{\rho_m W_G + \rho_G(1 - W_G)}, \tag{4}$$

in which W_G is the weight fraction of the graphene; ρ_G and ρ_m are the densities of graphene and matrix, respectively.

To determine the effective Young's modulus of the present panels, the modified Halpin-Tsai model (Halpin and Kardos 1976) and Voigt model (De Villoria and Miravete 2007) are employed as

$$E^{(i)} = \frac{3}{8}\frac{1 + 2A_G\eta_1 V_G^{(i)}}{1 - \eta_1 V_G^{(i)}} E^m + \frac{5}{8}\frac{1 + 2B_G\eta_2 V_G^{(i)}}{1 - \eta_2 V_G^{(i)}} E^m, \tag{5}$$

where $A_G = a_G/h_G$ and $B_G = b_G/h_G$, in which a_G, b_G and h_G are the length, width and thickness of the graphene platelets. The coefficients η_1 and η_2 are given as (Song *et al*. 2017, Feng *et al*. 2017)

$$\eta_1 = \frac{\frac{E^G}{E^m} - 1}{\frac{E^G}{E^m} + 2A_G}, \qquad \eta_2 = \frac{\frac{E^G}{E^m} - 1}{\frac{E^G}{E^m} + 2B_G}, \tag{6}$$

in which E^G and E^m are Young's moduli of the graphene platelets and polymer matrix, respectively. Similarly, the mass density $\rho^{(i)}$ and Poisson's ratio $\nu^{(i)}$ for ith layer are given by

$$\begin{aligned} \rho^{(i)} &= V_G^{(i)}\rho_G + \left(1 - V_G^{(i)}\right)\rho_m, \\ \nu^{(i)} &= V_G^{(i)}\nu_G + (1 - V_G^{(i)})\nu_m, \end{aligned} \tag{7}$$

where ν_G and ν_m are Poisson's ratios of platelets and matrix, respectively.

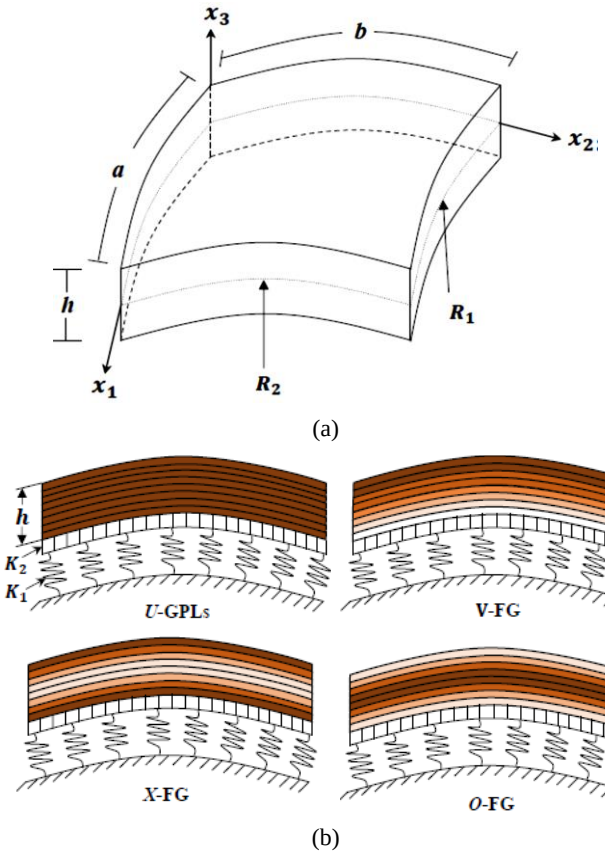

Fig. 1 (a) Geometrical dimensions and coordinates of a doubly-curved shell; and (b) various types of FGGPRC shells resting on elastic foundations

3. Basic equations

Based on the two-unknown shear deformation theory (TSDT) that was developed by Shimpi (2002), the proposed theory is established. The TSDT has been extended by many researchers to contain four unknowns and different shape functions (see, e.g., Benachour *et al*. 2011, Bourada *et al*. 2012, Thai and Vo 2013, Karami *et al*. 2018c, Sobhy and Zenkour 2019b). The displacement field, according to a novel four-variable shear deformation shell theory, is given as follows

$$u(\xi_1, \xi_2, \xi_3, t) = \left(1 + \frac{\xi_3}{R_1}\right)\mathcal{U}(\xi_1, \xi_2, t) - \xi_3\frac{\partial \mathcal{W}_b}{\varrho_1\,\partial\xi_1} - \frac{H(\xi_3)(\partial \mathcal{W}_s)}{\varrho_1\,\partial\xi_1}, \tag{8}$$

$$v(\xi_1,\xi_2,\xi_3,t)=\left(1+\frac{\xi_3}{R_2}\right)\mathcal{V}(\xi_1,\xi_2,t)-\xi_3\frac{\partial\mathcal{W}_b}{\varrho_2\,\partial\xi_2}-\frac{H(\xi_3)(\partial\mathcal{W}_s)}{\varrho_2\,\partial\xi_2},$$
$$w(\xi_1,\xi_2,\xi_3,t)=\mathcal{W}_b(\xi_1,\xi_2,t)+\mathcal{W}_s(\xi_1,\xi_2,t), \quad (8)$$

where $\mathcal{U}\$$ and $\mathcal{V}$ denote the longitudinal and latitudinal displacements of the middle plane, $\mathcal{W}_b$and $\mathcal{W}_s$ stand for the bending and shear deflections (Shimpi 2002), ϱ_j $(j=1,2)$ are the tangents to the ξ_j-axes, and the shape function $H(\xi_3)$ is expressed as (Sobhy 2016)

$$H(\xi_3)=\frac{4\xi_3^3}{3h^2}. \quad (9)$$

The non-zero strain-displacement relations, corresponding to the present four-variable shell theory, are obtained as (Reddy and Liu 1976)

$$\varepsilon_{11}=\epsilon_{11}^0+\xi_3\epsilon_{11}^b+H\epsilon_{11}^s,\quad \varepsilon_{22}=\epsilon_{22}^0+\xi_3\epsilon_{22}^b+H\epsilon_{22}^s,$$
$$\varepsilon_{12}=\epsilon_{12}^0+\xi_3\epsilon_{12}^b+H\epsilon_{12}^s,\quad \varepsilon_{23}=\overline{H}\epsilon_{23}^s,\quad \varepsilon_{13}=\overline{H}\epsilon_{13}^s, \quad (10)$$

where

$$\epsilon_{11}^0=\frac{\partial\mathcal{U}}{\partial x_1}+\frac{\mathcal{W}_b+\mathcal{W}_s}{R_1},\quad \epsilon_{22}^0=\frac{\partial\mathcal{V}}{\partial x_2}+\frac{\mathcal{W}_b+\mathcal{W}_s}{R_2},$$
$$\epsilon_{12}^0=\frac{\partial\mathcal{V}}{\partial x_1}+\frac{\partial\mathcal{U}}{\partial x_2},\quad \epsilon_{11}^b=-\frac{\partial^2\mathcal{W}_b}{\partial x_1^2},$$
$$\epsilon_{22}^b=-\frac{\partial^2\mathcal{W}_b}{\partial x_2^2},\quad \epsilon_{12}^b=-2\frac{\partial^2\mathcal{W}_b}{\partial x_1\,\partial x_2},$$
$$\epsilon_{11}^s=-\frac{\partial^2\mathcal{W}_s}{\partial x_1^2},\quad \epsilon_{22}^s=-\frac{\partial^2\mathcal{W}_s}{\partial x_2^2},$$
$$\epsilon_{12}^s=-2\frac{\partial^2\mathcal{W}_s}{\partial x_1\,\partial x_2},\quad \epsilon_{23}^s=\frac{\partial\mathcal{W}_s}{\partial x_2},$$
$$\epsilon_{13}^s=\frac{\partial\mathcal{W}_s}{\partial x_1},\quad \overline{H}=1-\frac{\mathrm{d}H}{\mathrm{d}\xi_3},$$
$$\mathrm{d}x_j=\varrho_j\mathrm{d}\xi_j,\quad j=1,2. \quad (11)$$

Each layer of the FGGPRC doubly-curved shallow shell is isotropic, therefore, the linear stress-strain relations for the ith layer are expressed by

$$\sigma_1^{(i)}=C_{11}^{(i)}\varepsilon_{11}+C_{12}^{(i)}\varepsilon_{22},\quad \sigma_2^{(i)}=C_{12}^{(i)}\varepsilon_{11}+C_{22}^{(i)}\varepsilon_{22},$$
$$\sigma_4^{(i)}=G_{23}^{(i)}\varepsilon_{23},\sigma_5^{(i)}=G_{13}^{(i)}\varepsilon_{13},\quad \sigma_6^{(i)}=G_{12}^{(i)}\varepsilon_{12}, \quad (12)$$

where

$$C_{11}^{(i)}=C_{22}^{(i)}=\frac{E^{(i)}}{1-(\nu^{(i)})^2},\quad C_{12}^{(i)}=\frac{\nu^{(i)}E^{(i)}}{1-(\nu^{(i)})^2},$$
$$G_{12}^{(i)}=G_{13}^{(i)}=G_{23}^{(i)}=\frac{E^{(i)}}{2(1+\nu^{(i)})}. \quad (13)$$

4. Equations of motion

The governing equations of motion can be derived by utilizing Hamilton's principle that expressed as

$$\int_0^t\delta(\Pi_s+\Pi_k-\Pi_f)\mathrm{d}t=0, \quad (14)$$

where Π_s stands for the strain energy and Π_k represents the kinetic energy, while, Π_f denotes the work done by the elastic foundations, which can be expressed as

$$\Pi_s=\frac{1}{2}\sum_{i=1}^{N}\int_V\left(\sigma_1^{(i)}\varepsilon_{11}+\sigma_2^{(i)}\varepsilon_{22}+\sigma_4^{(i)}\varepsilon_{23}+\sigma_5^{(i)}\varepsilon_{13}+\sigma_6^{(i)}\varepsilon_{12}\right)\mathrm{d}V, \quad (15)$$

$$\Pi_k=\frac{1}{2}\sum_{i=1}^{N}\int_V\rho^{(i)}(\dot{u}^2+\dot{v}^2+\dot{w}^2)\mathrm{d}V, \quad (16)$$

$$\Pi_f=-\frac{1}{2}\int_A\left\{K_1\,w^2-K_2\left[\left(\frac{\partial w}{\partial x_1}\right)^2+\left(\frac{\partial w}{\partial x_2}\right)^2\right]\right\}\mathrm{d}A, \quad (17)$$

where K_1 and K_2 are the elastic foundation stiffnesses. By substituting Eq. (10) into Eq. (15), one can obtain the variation of the strain energy $\delta\Pi_s$ as

$$\delta\Pi_s=\int_A(N_1\,\epsilon_{11}^0+M_1\epsilon_{11}^b+\bar{M}_1\epsilon_{11}^s+N_2\epsilon_{22}^0+M_2\epsilon_{22}^b+\bar{M}_2\epsilon_{22}^s+N_6\epsilon_{12}^0+M_6\epsilon_{12}^b+\bar{M}_6\epsilon_{12}^s+S_4\epsilon_{23}^s+S_5\epsilon_{13}^s)\mathrm{d}V, \quad (18)$$

where N_j $(j=1,2,6)$ are the stress resultants; M_j and $\bar{M}_j$ are the moment and additional moment resultants; Q_j $(j=4,5)$ are the resultants of transverse shear stresses, which are given as

$$\{N_j,M_j,\bar{M}_j\}=\sum_{i=1}^{N}\int_{h_i}^{h_{i+1}}\sigma_j^{(i)}\{1,\xi_3,H(\xi_3)\}\mathrm{d}\xi_3,$$
$$Q_r=\sum_{i=1}^{N}\int_{h_i}^{h_{i+1}}\sigma_r^{(i)}\overline{H}(\xi_3)\mathrm{d}\xi_3, \quad (19)$$
$$j=1,2,6,\quad r=4,5,\quad h_1=-\frac{h}{2},\quad h_{N+1}=\frac{h}{2},$$

where $\xi_3=h_i$ and $\xi_3=h_{i+1}$ are, respectively, the coordinates of the lower and upper surfaces of the ith composite layer. The coordinates h_k can be calculated by

$$h_k=-\left(\frac{N}{2}-k+1\right)\frac{h}{N},\quad k=1,2,3,\dots,N+1. \quad (20)$$

By inserting Eqs. (16)-(18) into Eq. (14) with the aid of Eq. (8) and integrating by parts, the coefficients of $\delta\mathcal{U}$, $\delta\mathcal{V}$, $\delta\mathcal{W}_b$ and $\delta\mathcal{W}_s$ can be obtained as follows

$$\frac{\partial N_1}{\partial x_1}+\frac{\partial N_6}{\partial x_2}=\bar{J}_{11}\,\ddot{\mathcal{U}}-\bar{J}_{12}\frac{\partial \ddot{\mathcal{W}}_b}{\partial x_1}-\bar{J}_{13}\frac{\partial \ddot{\mathcal{W}}_s}{\partial x_1},$$

$$\frac{\partial N_6}{\partial x_1}+\frac{\partial N_2}{\partial x_2}=\bar{J}'_{11}\,\ddot{\mathcal{V}}-\bar{J}'_{12}\frac{\partial \ddot{\mathcal{W}}_b}{\partial x_2}-\bar{J}'_{13}\frac{\partial \ddot{\mathcal{W}}_s}{\partial x_2},$$

$$\begin{aligned}&\frac{\partial^2 M_1}{\partial x_1^2}+2\frac{\partial^2 M_6}{\partial x_1\,\partial x_2}+\frac{\partial^2 M_2}{\partial x_2^2}-\frac{N_1}{R_1}-\frac{N_2}{R_2}\\&-K_1(\mathcal{W}_b+\mathcal{W}_s)+K_2\nabla^2(\mathcal{W}_b+\mathcal{W}_s)\\&=\bar{J}_{21}\big(\ddot{\mathcal{W}}_b+\ddot{\mathcal{W}}_s\big)+\bar{J}_{12}\frac{\partial\,\ddot{\mathcal{U}}}{\partial x_1}+\bar{J}'_{12}\frac{\partial\,\ddot{\mathcal{V}}}{\partial x_2}\\&-\bar{J}_{22}\nabla^2\ddot{\mathcal{W}}_b-\bar{J}_{23}\nabla^2\ddot{\mathcal{W}}_s,\end{aligned}\tag{21}$$

$$\begin{aligned}&\frac{\partial^2 \overline{M}_1}{\partial x_1^2}+2\frac{\partial^2 \overline{M}_6}{\partial x_1\,\partial x_2}+\frac{\partial^2 \overline{M}_2}{\partial x_2^2}+\frac{\partial S_4}{\partial x_2}+\frac{\partial S_5}{\partial x_1}\\&-\frac{N_1}{R_1}-\frac{N_2}{R_2}-K_1(\mathcal{W}_b+\mathcal{W}_s)+K_2\nabla^2(\mathcal{W}_b+\mathcal{W}_s)\\&=\bar{J}_{21}\big(\ddot{\mathcal{W}}_b+\ddot{\mathcal{W}}_s\big)+\bar{J}_{13}\frac{\partial\,\ddot{\mathcal{U}}}{\partial x_1}+\bar{J}'_{13}\frac{\partial\,\ddot{\mathcal{V}}}{\partial x_2}\\&-\bar{J}_{23}\nabla^2\ddot{\mathcal{W}}_b-\bar{J}_{33}\nabla^2\ddot{\mathcal{W}}_s,\end{aligned}$$

where $\bar{J}_{jk}$ are the inertias that can be expressed as

$$\begin{aligned}&\bar{J}_{11}=J_1+\frac{2J_2}{R_1}, && \bar{J}'_{11}=J_1+\frac{2J_2}{R_2},\\&\bar{J}_{12}=J_2+\frac{J_3}{R_1}, && \bar{J}'_{12}=J_2+\frac{J_3}{R_2},\\&\bar{J}_{13}=J_4+\frac{J_5}{R_1}, && \bar{J}'_{13}=J_4+\frac{J_5}{R_2},\\&\bar{J}_{21}=J_1, && \bar{J}_{22}=J_3,\\&\bar{J}_{23}=J_5, && \bar{J}_{33}=J_6,\end{aligned}\tag{22}$$

where

$$\begin{aligned}&\{J_1,J_2,J_3,J_4,J_5,J_6\}\\&=\sum_{i=1}^{N}\int_{h_i}^{h_{i+1}}\rho^{(i)}\{1,\xi_3,\xi_3^2,H(\xi_3),\xi_3H(\xi_3),H^2(\xi_3)\}\mathrm{d}\xi_3.\end{aligned}\tag{23}$$

Inserting Eq. (10) into Eq. (12) and substituting the resulting equation into Eq. (19) give

$$\begin{aligned}N_1&=A_{11}\epsilon_{11}^0+A_{12}\epsilon_{11}^b+A_{13}\epsilon_{11}^s\\&\quad+B_{11}\epsilon_{22}^0+B_{12}\epsilon_{22}^b+B_{13}\epsilon_{22}^s,\\N_2&=B_{11}\epsilon_{11}^0+B_{12}\epsilon_{11}^b+B_{13}\epsilon_{11}^s\\&\quad+A_{11}\epsilon_{22}^0+A_{12}\epsilon_{22}^b+A_{13}\epsilon_{22}^s,\\N_6&=D_{11}\epsilon_{12}^0+D_{12}\epsilon_{12}^b+D_{13}\epsilon_{12}^s,\\M_1&=A_{12}\epsilon_{11}^0+A_{22}\epsilon_{11}^b+A_{23}\epsilon_{11}^s\\&\quad+B_{12}\epsilon_{22}^0+B_{22}\epsilon_{22}^b+B_{23}\epsilon_{22}^s,\\M_2&=B_{12}\epsilon_{11}^0+B_{22}\epsilon_{11}^b+B_{23}\epsilon_{11}^s\\&\quad+A_{12}\epsilon_{22}^0+A_{22}\epsilon_{22}^b+A_{23}\epsilon_{22}^s,\\M_6&=D_{12}\epsilon_{12}^0+D_{22}\epsilon_{12}^b+D_{23}\epsilon_{12}^s,\\\overline{M}_1&=A_{13}\epsilon_{11}^0+A_{23}\epsilon_{11}^b+A_{33}\epsilon_{11}^s\\&\quad+B_{13}\epsilon_{22}^0+B_{23}\epsilon_{22}^b+B_{33}\epsilon_{22}^s,\\\overline{M}_2&=B_{13}\epsilon_{11}^0+B_{23}\epsilon_{11}^b+B_{33}\epsilon_{11}^s\\&\quad+A_{13}\epsilon_{22}^0+A_{23}\epsilon_{22}^b+A_{33}\epsilon_{22}^s,\\\overline{M}_6&=D_{13}\epsilon_{12}^0+D_{23}\epsilon_{12}^b+D_{33}\epsilon_{12}^s,\\Q_4&=A_{44}\epsilon_{23}^s,\qquad Q_5=A_{55}\epsilon_{13}^s,\end{aligned}\tag{24}$$

where

$$\begin{aligned}\{A_{11},A_{12},A_{13},A_{22},A_{23},A_{33}\}&=\sum_{i=1}^{N}\int_{h_i}^{h_{i+1}}C_{11}^{(i)}\Xi\mathrm{d}\xi_3,\\\{B_{11},B_{12},B_{13},B_{22},B_{23},B_{33}\}&=\sum_{i=1}^{N}\int_{h_i}^{h_{i+1}}C_{12}^{(i)}\Xi\mathrm{d}\xi_3,\\\{D_{11},D_{12},D_{13},D_{22},D_{23},D_{33}\}&=\sum_{i=1}^{N}\int_{h_i}^{h_{i+1}}G_{12}^{(i)}\Xi\mathrm{d}\xi_3,\\\{A_{44},A_{55}\}&=\sum_{i=1}^{N}\int_{h_i}^{h_{i+1}}\overline{H}^2(\xi_3)\big\{G_{23}^{(i)},G_{13}^{(i)}\big\}\mathrm{d}\xi_3,\\\Xi&=\{1,\xi_3,H(\xi_3),\xi_3^2,\xi_3H(\xi_3),H^2(\xi_3)\}.\end{aligned}\tag{25}$$

5. Analytical solutions

In this section, the motion governing equations are analytically solved to obtain the eigenfrequency of the FGGPRC doubly-curved shallow shells resting on elastic foundations. The boundary conditions in x_1 direction are given as:

Simply-supported/Simply-supported (SS):

$$\begin{aligned}&\mathcal{V}=\mathcal{W}_b=\mathcal{W}_s=\frac{\partial \mathcal{W}_b}{\partial x_2}=\frac{\partial \mathcal{W}_s}{\partial x_2}\\&=N_1=M_1=\overline{M}_1=0,\quad\text{at}\quad x_1=0,a,\end{aligned}\tag{26}$$

Clamped/Simply-supported (CS):

$$\begin{aligned}&\mathcal{U}=\mathcal{V}=\mathcal{W}_b=\mathcal{W}_s\\&=\frac{\partial \mathcal{W}_b}{\partial x_1}=\frac{\partial \mathcal{W}_b}{\partial x_2}=\frac{\partial \mathcal{W}_s}{\partial x_1}=\frac{\partial \mathcal{W}_s}{\partial x_2}=0,\ \text{at}\ \ x_1=0,\\&\mathcal{V}=\mathcal{W}_b=\mathcal{W}_s\\&=\frac{\partial \mathcal{W}_b}{\partial x_2}=\frac{\partial \mathcal{W}_s}{\partial x_2}=N_1=M_1=\overline{M}_1,\ \text{at}\ \ x_1=a,\end{aligned}\tag{27}$$

Clamped/Clamped (CC):

$$\begin{aligned}&\mathcal{U}=\mathcal{V}=\mathcal{W}_b=\mathcal{W}_s\\&=\frac{\partial \mathcal{W}_b}{\partial x_1}=\frac{\partial \mathcal{W}_b}{\partial x_2}=\frac{\partial \mathcal{W}_s}{\partial x_1}=\frac{\partial \mathcal{W}_s}{\partial x_2}=0,\ \text{at}\ \ x_1=0,a.\end{aligned}\tag{28}$$

Table 1 The functions $\Gamma_n(x_1)$ and $\Upsilon_r(x_2)$

B.C.	$\Gamma_n(x_1)$	$\Upsilon_r(x_2)$
SSSS	$\sin(\alpha x_1)$	$\sin(\beta x_2)$
CSSS	$\sin(\alpha x_1)\,[1-\cos(\alpha x_1)]$	$\sin(\beta x_2)$
CSCS	$\sin(\alpha x_1)\,[1-\cos(\alpha x_1)]$	$\sin(\beta x_2)\,[1-\cos(\beta x_2)]$
CCCS	$\sin^2(\alpha x_1)$	$\sin(\beta x_2)\,[1-\cos(\beta x_2)]$
CCCC	$\sin^2(\alpha x_1)$	$\sin^2(\beta x_2)$

Similarly, the boundary conditions in x_2 direction can be given.

Reddy and Liu (1976) presented the solution of the motion equations for laminated shells employing Navier's type method. However, Navier's method is only appropriate for the simply-supported shells. Therefore, the displacements are represented by the trigonometric functions (Sobhy 2013, 2014a, b, Thai *et al*. 2014, Meziane *et al*. 2014) to satisfy the different boundary conditions as

$$\begin{aligned}
\mathcal{U} &= \sum_{n=1}^{\infty}\sum_{r=1}^{\infty} \tilde{\mathcal{U}}_{nr}\exp(I\omega_{nr}\,t)\frac{\mathrm{d}\Gamma_n(x_1)}{\mathrm{d}x_1}\,\Upsilon_r\,(x_2)\,,\\
\mathcal{V} &= \sum_{n=1}^{\infty}\sum_{r=1}^{\infty} \tilde{\mathcal{V}}_{nr}\exp(I\omega_{nr}t)\;\Gamma_n(x_1)\frac{\mathrm{d}\Upsilon_r(x_2)}{\mathrm{d}x_2},\\
\mathcal{W}_b &= \sum_{n=1}^{\infty}\sum_{r=1}^{\infty} \tilde{\mathcal{W}}^b_{nr}\exp(I\omega_{nr}t)\,\Gamma_n(x_1)\Upsilon_r(x_2)\,,\\
\mathcal{W}_s &= \sum_{n=1}^{\infty}\sum_{r=1}^{\infty} \tilde{\mathcal{W}}^s_{nr}\exp(I\omega_{nr}t)\,\Gamma_n(x_1)\Upsilon_r(x_2),
\end{aligned} \tag{29}$$

where $I=\sqrt{-1}$, $\omega=\omega_{nr}$ is the eigenfrequency, (n,r) are the mode numbers, $(\tilde{\mathcal{U}},\tilde{\mathcal{V}},\mathcal{W}^b_{nr},\mathcal{W}^s_{nr})$ are unknown functions that will be determined, and the functions $\Gamma_n(x_1)$ and $\Upsilon_r(x_2)$ are shown in Table 1 noting that $\alpha=n\pi/a$ and $\beta=r\pi/b$.

By incorporating Eq. (29) into Eq. (21) with the aid of Eqs. (11) and (24), one can obtain the equations of motion of the FGGPRC doubly-curved shallow shells in terms of the parameters $(\tilde{\mathcal{U}},\tilde{\mathcal{V}},\mathcal{W}^b_{nr},\mathcal{W}^s_{nr})$ as

$$\begin{bmatrix} \Phi_{11} & \Phi_{12} & \Phi_{13} & \Phi_{14}\\ & \Phi_{22} & \Phi_{23} & \Phi_{24}\\ & & \Phi_{33} & \Phi_{34}\\ \text{symm.} & & & \Phi_{44}\end{bmatrix} - \omega^2\begin{bmatrix} \Psi_{11} & \Psi_{12} & \Psi_{13} & \Psi_{14}\\ & \Psi_{22} & \Psi_{23} & \Psi_{24}\\ & & \Psi_{33} & \Psi_{34}\\ \text{symm.} & & & \Psi_{44}\end{bmatrix}\begin{Bmatrix}\tilde{\mathcal{U}}_{nr}\\ \tilde{\mathcal{V}}_{nr}\\ \tilde{\mathcal{W}}^b_{nr}\\ \tilde{\mathcal{W}}^s_{nr}\end{Bmatrix} = 0, \tag{30}$$

where the elements Φ_{ij} and Ψ_{ij} are given as

$$\begin{aligned}
\Phi_{11} &= A_{11}\varsigma_{13}+D_{11}\varsigma_{12},\\
\Phi_{12} &= (B_{11}+D_{11})\varsigma_{12},\\
\Phi_{13} &= \left(\frac{A_{11}}{R_1}+\frac{B_{11}}{R_2}\right)\varsigma_{11}-(B_{12}+2D_{12})\varsigma_{12}-A_{12}\varsigma_{13},\\
\Phi_{14} &= \left(\frac{A_{11}}{R_1}+\frac{B_{11}}{R_2}\right)\varsigma_{11}-(B_{13}+2D_{13})\varsigma_{12}-A_{13}\varsigma_{13},\\
\Phi_{21} &= (B_{11}+D_{11})\varsigma_{23},\\
\Phi_{22} &= A_{11}\varsigma_{22}+D_{11}\varsigma_{23},\\
\Phi_{23} &= \left(\frac{B_{11}}{R_1}+\frac{A_{11}}{R_2}\right)\varsigma_{21}-(B_{12}+2D_{12})\varsigma_{23}-A_{12}\varsigma_{22},\\
\Phi_{24} &= \left(\frac{B_{11}}{R_1}+\frac{A_{11}}{R_2}\right)\varsigma_{21}-(B_{13}+2D_{13})\varsigma_{23}-A_{13}\varsigma_{22},\\
\Phi_{31} &= -\left(\frac{A_{11}}{R_1}+\frac{B_{11}}{R_2}\right)\varsigma_{34}+(B_{12}+2D_{12})\varsigma_{35}+A_{12}\varsigma_{36}\\
\Phi_{32} &= -\left(\frac{B_{11}}{R_1}+\frac{A_{11}}{R_2}\right)\varsigma_{32}+(B_{12}+2D_{12})\varsigma_{35}+A_{12}\varsigma_{33},\\
\Phi_{33} &= 2\frac{A_{12}\varsigma_{34}+B_{12}\varsigma_{32}}{R_1}+2\frac{B_{12}\varsigma_{34}+A_{12}\varsigma_{32}}{R_2}\\
&\quad -\left(K_1+\frac{A_{11}}{R_1^2}+2\frac{B_{11}}{R_1R_2}+\frac{A_{11}}{R_2^2}\right)\varsigma_{31}\\
&\quad -2(B_{22}+2D_{22})\varsigma_{35}-A_{22}\varsigma_{36}-A_{22}\varsigma_{33}\\
&\quad +K_2(\varsigma_{32}+\varsigma_{34}),\\
\Phi_{34} &= \frac{(A_{12}+A_{13})\varsigma_{34}+(B_{12}+B_{13})\varsigma_{32}}{R_1}\\
&\quad +\frac{(B_{12}+B_{13})\varsigma_{34}+(A_{12}+A_{13})\varsigma_{32}}{R_2}\\
&\quad -\left(K_1+\frac{A_{11}}{R_1^2}+2\frac{B_{11}}{R_1R_2}+\frac{A_{11}}{R_2^2}\right)\varsigma_{31}\\
&\quad -2(B_{23}+2D_{23})\varsigma_{35}-A_{23}\varsigma_{36}-A_{23}\varsigma_{33}\\
&\quad +K_2(\varsigma_{32}+\varsigma_{34}),\\
\Phi_{41} &= -\left(\frac{A_{11}}{R_1}+\frac{B_{11}}{R_2}\right)\varsigma_{34}+(B_{13}+2D_{13})\varsigma_{35}+A_{13}\varsigma_{36},\\
\Phi_{42} &= -\left(\frac{B_{11}}{R_1}+\frac{A_{11}}{R_2}\right)\varsigma_{32}+(B_{13}+2D_{13})\varsigma_{35}+A_{13}\varsigma_{33},\\
\Phi_{43} &= \Phi_{34},\\
\Phi_{44} &= 2\frac{A_{13}\varsigma_{34}+B_{13}\varsigma_{32}}{R_1}+2\frac{B_{13}\varsigma_{34}+A_{13}\varsigma_{32}}{R_2}\\
&\quad -\left(K_1+\frac{A_{11}}{R_1^2}+2\frac{B_{11}}{R_1R_2}+\frac{A_{11}}{R_2^2}\right)\varsigma_{31}\\
&\quad -2(B_{33}+2D_{33})\varsigma_{35}-A_{33}\varsigma_{36}-A_{33}\varsigma_{33}\\
&\quad +A_{44}\varsigma_{32}+A_{55}\varsigma_{34}+K_2(\varsigma_{32}+\varsigma_{34}),
\end{aligned} \tag{31}$$

$$\begin{aligned}
&\Psi_{11}=-\bar{J}_{11}\varsigma_{11}, && \Psi_{12}=0,\\
&\Psi_{13}=\bar{J}_{12}\varsigma_{11}, && \Psi_{14}=\bar{J}_{13}\varsigma_{11},\\
&\Psi_{21}=0, && \Psi_{22}=-\bar{J}'_{11}\varsigma_{21},\\
&\Psi_{23}=\bar{J}'_{12}\varsigma_{21}, && \Psi_{14}=\bar{J}'_{13}\varsigma_{21},\\
&\Psi_{31}=-\bar{J}_{12}\varsigma_{34}, && \Psi_{32}=-\bar{J}'_{12}\varsigma_{32},\\
&\Psi_{33}=-\bar{J}_{21}\varsigma_{31}+\bar{J}_{22}(\varsigma_{32}+\varsigma_{34}),\\
&\Psi_{34}=-\bar{J}_{21}\varsigma_{31}+\bar{J}_{23}(\varsigma_{32}+\varsigma_{34}),\\
&\Psi_{41}=-\bar{J}_{13}\varsigma_{34}, && \Psi_{42}=-\bar{J}'_{13}\varsigma_{32},\\
&\Psi_{43}=-\bar{J}_{21}\varsigma_{31}+\bar{J}_{23}(\varsigma_{32}+\varsigma_{34}),\\
&\Psi_{44}=-\bar{J}_{21}\varsigma_{31}+\bar{J}_{33}(\varsigma_{32}+\varsigma_{34}),
\end{aligned} \tag{32}$$

in which

$$(\varsigma_{11},\varsigma_{12})=\int_0^b\int_0^a\left(\Upsilon_r(x_2),\frac{\mathrm{d}^2\Upsilon_r(x_2)}{\mathrm{d}x_2^2}\right)\left(\frac{\mathrm{d}\Gamma_n(x_1)}{\mathrm{d}x_1}\right)^2\times\Upsilon_r(x_2)\mathrm{d}x_1\mathrm{d}x_2,$$

$$(\varsigma_{13},\varsigma_{36})=\int_0^b\int_0^a\left(\frac{\mathrm{d}^3\Gamma_n(x_1)}{\mathrm{d}x_1^3}\frac{\mathrm{d}\Gamma_n(x_1)}{\mathrm{d}x_1},\frac{\mathrm{d}^4\Gamma_n(x_1)}{\mathrm{d}x_1^4}\Gamma_n(x_1)\right)\times\Upsilon_r^2(x_2)\mathrm{d}x_1\mathrm{d}x_2,$$

$$(\varsigma_{21},\varsigma_{22})=\int_0^b\int_0^a\left(\frac{\mathrm{d}\Upsilon_r(x_2)}{\mathrm{d}x_2},\frac{\mathrm{d}^3\Upsilon_r(x_2)}{\mathrm{d}x_2^3}\right)\Gamma_n^2(x_1)\times\frac{\mathrm{d}\Upsilon_r(x_2)}{\mathrm{d}x_2}\mathrm{d}x_1\mathrm{d}x_2,\tag{33}$$

$$\varsigma_{23}=\int_0^b\int_0^a\Gamma_n(x_1)\frac{\mathrm{d}^2\Gamma_n(x_1)}{\mathrm{d}x_1^2}\left(\frac{\mathrm{d}\Upsilon_r(x_2)}{\mathrm{d}x_2}\right)^2\mathrm{d}x_1\mathrm{d}x_2,$$

$$(\varsigma_{31},\varsigma_{32},\varsigma_{33})=\int_0^b\int_0^a\left(\Upsilon_r(x_2),\frac{\mathrm{d}^2\Upsilon_r(x_2)}{\mathrm{d}x_2^2},\frac{\mathrm{d}^4\Upsilon_r(x_2)}{\mathrm{d}x_2^4}\right)\times\Gamma_n^2(x_1)\Upsilon_r(x_2)\mathrm{d}x_1\mathrm{d}x_2,$$

$$(\varsigma_{34},\varsigma_{35})=\int_0^b\int_0^a\left(\Upsilon_r^2(x_2),\Upsilon_r(x_2)\frac{\mathrm{d}^2\Upsilon_r(x_2)}{\mathrm{d}x_2^2}\right)\times\Gamma_n(x_1)\frac{\mathrm{d}^2\Gamma_n(x_1)}{\mathrm{d}x_1^2}\mathrm{d}x_1\mathrm{d}x_2.\tag{33}$$

In order to calculate the natural frequencies of the FGGPRC doubly-curved shallow shells, the eigenvalue problem (30) should be solved.

6. Numerical results

In this section, some numerical results for the free vibration analysis of the different types of FGGPRC doubly-curved shells with several boundary conditions are discussed. The following data is used in the present numerical calculations: $V_{min}=\frac{V_G^*}{5}$, $N=10, a_G=2.5\,\mu$m, $b_G=1.5\,\mu$m, $h_G=1.5$ nm. The material properties of the graphene platelets and epoxy matrix are given as (Song *et al.* 2017): $E^G=1.01$ TPa, $\rho_G=1060$ kg/m^3, $\nu_G=0.186, E^m=3$ GPa, $\rho_m=1200$ kg/m^3, $\nu_m=0.34$.

Table 2 Comparison of nondimensional frequency $\omega a^2\sqrt{\rho h/D}$ of different types of SSSS homogeneous shallow shells ($a/h=20,\ \ a=b,\ \ \nu=0.3,\ \ \bar{K}_1=\bar{K}_2=0$)

a/R_1	Source	Spherical shell ($R_1/R_2=1$)	Cylindrical shell ($R_1/R_2=0$)	Hyperbolic paraboloidal shell ($R_1/R_2=-1$)
0.5	Qatu and Asadi (2012)	38.01	25.48	19.25
	Ghavanloo and Fazelzadeh (2013)	37.9698	25.3508	18.7628
	Present	37.9391	25.3562	19.0836
0.2	Qatu and Asadi (2012)	23.70	20.78	19.66
	Ghavanloo and Fazelzadeh (2013)	23.6867	20.7543	19.5783
	Present	23.5547	20.6148	19.4834

Table 3 Comparison of nondimensional frequency $\omega h\sqrt{\rho_c/E_c}$ of different types of SSSS FG shallow shells ($a/h=10,\ a=b,\ \bar{K}_1=\bar{K}_2=0$)

a/R_1	R_1/R_2	k	Matsunaga (2008)	Chorfi and Houmat (2010)	Pouresmaeeli and Fazelzadeh (2016)	mPresent
0.5	1	0	0.0751	0.0762	0.0746	0.0753
		0.5	0.0657	0.0664	0.0646	0.0653
		1	0.0601	0.0607	0.0588	0.0594
		10	0.0464	0.0471	0.0455	0.0459
0.5	0	0	0.0622	0.0629	0.0616	0.0622
		0.5	0.0535	0.0540	0.0527	0.0532
		1	0.0485	0.0490	0.0477	0.0482
		10	0.0390	0.0395	0.0384	0.0387
0	0	0	0.0578	0.0577	0.0577	0.0577
		0.5	0.0492	0.0490	0.0490	0.0490
		1	0.0443	0.0442	0.0442	0.0442
		10	0.0364	0.0366	0.0366	0.0363

Table 4 Natural frequency $\omega*$ of U-GPLs composite doubly-curved shallow shells for various mode numbers (n,r) and side-to-thickness ratio a/h ($\frac{a}{R_1}=0.5,\ \frac{R_1}{R_2}=1,\ a=b,\ k=1,\ \overline{K}_1=100,\ \overline{K}_2=10,\ W_G=30\%$)

Mode (n,r)	a/h							
	5	10	15	20	25	30	35	40
(1,1)	23.6860	11.2988	5.63505	3.66417	2.69434	2.12536	1.75351	1.49215
(1,2)	48.2750	14.9123	7.33369	4.50570	3.14694	2.38408	1.90788	1.58692
(2,2)	69.1838	22.1500	10.7515	6.41019	4.32184	3.16049	2.44723	1.97624
(1,3)	81.5927	26.7769	13.0382	7.72886	5.15982	3.72922	2.85194	2.27473
(2,3)	98.5106	33.4025	16.4153	9.71832	6.44657	4.61665	3.49303	2.75434
(3,3)	123.400	43.6890	21.8524	12.9992	8.60784	6.13100	4.60320	3.59660
(3,4)	153.516	56.7882	29.0542	17.4586	11.6000	8.25848	6.18289	4.80936
(1,5)	157.482	58.5554	30.0463	18.0816	12.0221	8.56084	6.40876	4.98369
(2,5)	168.975	63.7207	32.9716	19.9299	13.2797	9.46431	7.08530	5.50695
(5,5)	237.420	95.4514	51.6310	32.0568	21.6983	15.6022	11.7337	9.13537

Table 5 Fundamental frequency ω^* of various types of SSSS FG graphene platelet-reinforced composite doubly-curved shallow shells on elastic foundations (a/h = 10, a = b, k = 1, WG = 30%, n = r = 1)

Type	$\frac{a}{R_1}$	$\frac{R_1}{R_2}$	$\overline{K}_1=100$				$\overline{K}_2=10$			
			$\overline{K}_2=0$	$\overline{K}_2=50$	$\overline{K}_2=100$	$\overline{K}_2=200$	$\overline{K}_1=0$	$\overline{K}_1=10$	$\overline{K}_1=100$	$\overline{K}_1=1000$
U-GPLs	0.5	1	7.71524	7.77546	7.83521	7.95336	7.72121	7.72182	7.72732	7.78217
	0.5	-1	5.75954	5.83752	5.91446	6.06539	5.76728	5.76808	5.77522	5.84618
	0.5	0	6.37263	6.44558	6.51771	6.65962	6.37987	6.38061	6.38729	6.45369
	0	0	5.90531	5.98543	6.06450	6.21961	5.91326	5.91408	5.92142	5.99433
X-FG	0.5	1	6.47207	6.54268	6.61253	6.75006	6.47907	6.47979	6.48625	6.55053
	0.5	-1	5.11535	5.20162	5.28646	5.45213	5.12393	5.12481	5.13272	5.21118
	0.5	0	5.54764	5.63006	5.71128	5.87035	5.55583	5.55667	5.56422	5.63921
	0	0	5.24712	5.33587	5.42318	5.59370	5.25594	5.25685	5.26499	5.34571
V -FG	0.5	1	5.55757	5.63807	5.71744	5.87294	5.56556	5.56638	5.57376	5.64701
	0.5	-1	4.04935	4.15758	4.26304	4.46644	4.06016	4.06127	4.07123	4.16951
	0.5	0	4.50655	4.60651	4.70434	4.89411	4.51652	4.51754	4.52672	4.61756
	0	0	4.15086	4.26200	4.37032	4.57928	4.16196	4.16310	4.17333	4.27426
O-FG	0.5	1	5.24758	5.33426	5.41955	5.58622	5.25620	5.25709	5.26503	5.34387
	0.5	-1	3.50484	3.62970	3.75038	3.98071	3.51736	3.51864	3.53017	3.64340
	0.5	0	4.05120	4.16319	4.27225	4.48238	4.06239	4.06353	4.07384	4.17554
	0	0	3.59206	3.72020	3.84407	4.08055	3.60491	3.60623	3.61805	3.73427

In the following, the used nondimensionalized parameters are presented as

$$\omega^* = 10h\omega\sqrt{\frac{\rho_m}{E^m}}, \qquad \overline{K}_1 = \frac{K_1 a^4}{D^m}, \qquad \overline{K}_2 = \frac{K_2 a^2}{D^m}, \qquad D^m = \frac{E^m h^3}{12[1-(\nu_m)^2]}. \tag{34}$$

As a validation example, the present frequencies are compared with those of Qatu and Asadi (2012) and Ghavanloo and Fazelzadeh (2013) in Table 2. Additional validation example is reported in Table 3 to compare the present frequencies with those given in Refs. (Matsunaga 2008, Chorfi and Houmat 2010, Pouresmaeeli and Fazelzadeh 2016). Table 2 shows that the present frequencies are in close agreement with whose in Qatu and Asadi (2012) and Ghavanloo and Fazelzadeh (2013) for different spherical, cylindrical, and hyperbolic paraboloidal shells. The frequencies increase as the shallowness ratio a/R_1 increases for the spherical and cylindrical shells and as a/R_1 decreases for the hyperbolic paraboloidal shell.

Once again, it is appeared from Table 3 that the present frequencies are in close agreement with whose in Refs. (Matsunaga 2008, Chorfi and Houmat 2010, Pouresmaeeli and Fazelzadeh 2016) for both FG spherical $(R_1/R_2=1)$ and cylindrical $(R_1/R_2=0)$ shells and also for the FG flat

Table 6 Fundamental frequency ω^* of various types of FG graphene platelet-reinforced composite doubly-curved shallow shells for different boundary conditions (a/h = 10, a = b, k = 1, $\overline{K}_1 = \overline{K}_2 = 0$, WG = 30%, n = r = 1)

Type	$\frac{a}{R_1}$	$\frac{R_1}{R_2}$	SSSS	CSSS	CSCS	CCCS	CCCC
U -GPLs	0.5	1	7.70912	9.98563	11.92867	12.25818	12.73471
	0.5	-1	5.75158	8.92519	11.12808	11.56343	11.94573
	0.5	0	6.36520	8.98980	10.96775	11.38849	11.53227
	0	0	5.89713	8.30459	10.36406	10.49397	10.65275
X-FG	0.5	1	6.46487	8.43458	10.09313	10.30859	10.62826
	0.5	-1	5.10653	7.69183	9.52797	9.81078	10.04963
	0.5	0	5.53922	7.75219	9.42475	9.69790	9.76979
	0	0	5.23804	7.28833	9.01448	9.08033	9.15849
V -FG	0.5	1	5.54935	7.15097	8.51543	8.79037	9.18957
	0.5	-1	4.03822	6.37585	7.93471	8.28412	8.57690
	0.5	0	4.49630	6.38006	7.76157	8.10644	8.22085
	0	0	4.13943	5.83939	7.29672	7.39648	7.51871
O-FG	0.5	1	5.23872	6.63842	7.82902	8.10642	8.50957
	0.5	-1	3.49194	5.68604	7.09605	7.46211	7.77567
	0.5	0	4.03968	5.72946	6.94139	7.30304	7.41026
	0	0	3.57882	5.07267	6.36235	6.46127	6.58380

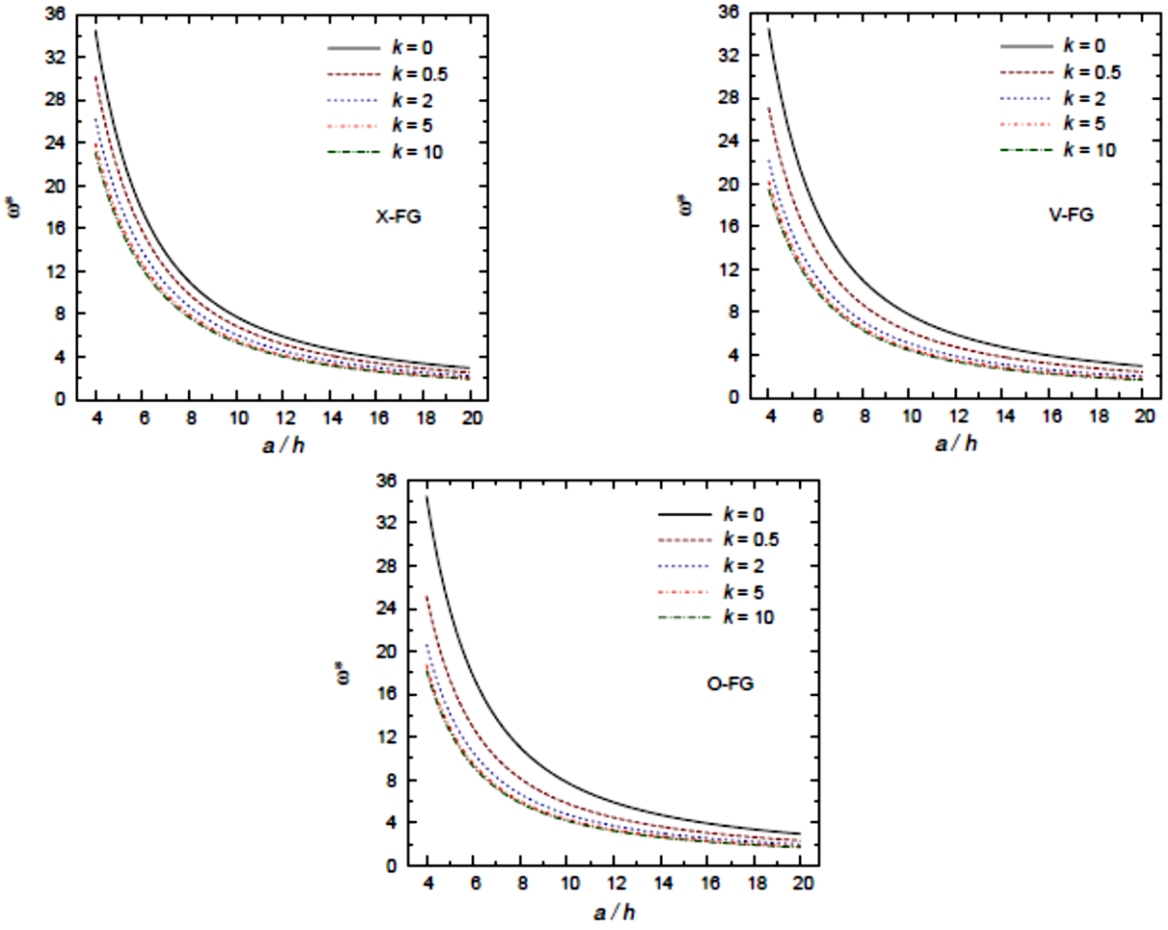

Fig. 2 Effects of power law index k on the frequency ω^* of various types of SSSS shallow shells (a) X-FG; (b) V-FG; and (c) O-FG $(a/R_1 = 0.5, R_1/R_2 = 1, a = b, \overline{K}_1 = 100, \overline{K}_2 = 50, W_G = 30\%, n = r = 1)$

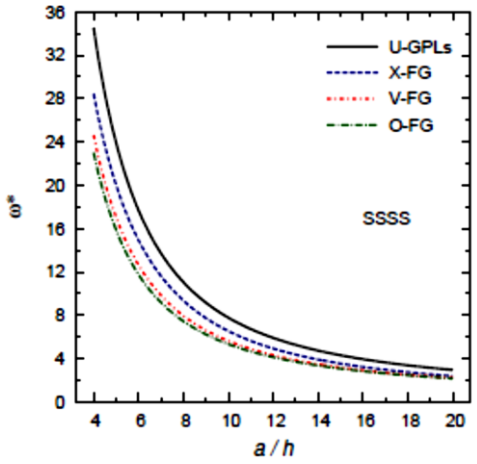

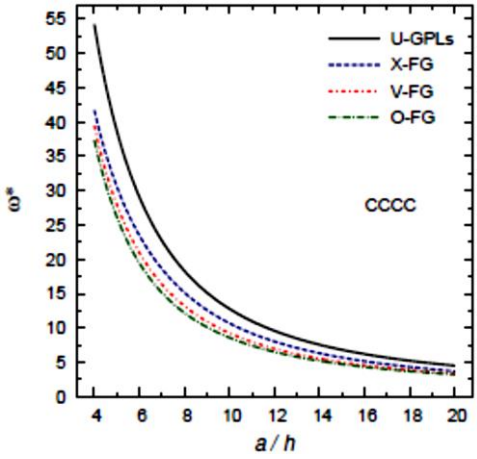

Fig. 3 Frequency ω^* of various types of (a) SSSS and (b) CCCC shallow shells $\left(k=1, a/R_1=0.5, R_1/R_2=1, a=b, \overline{K}_1=100, \overline{K}_2=50, W_G=30\%, n=r=1\right)$

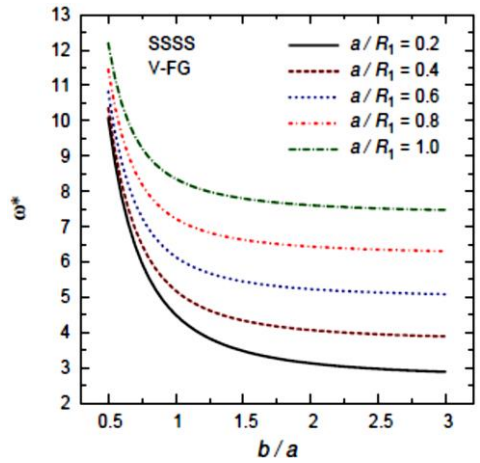

Fig. 4 Effects of shallowness ratio a/R_1 on the frequency ω^* of an SSSS shallow shell $(k=1,\ R_1/R_2=1,\ a/h=10,\ \overline{K}_1=100,\ \overline{K}_2=50,\ W_G=30\%,\ n=r=1)$

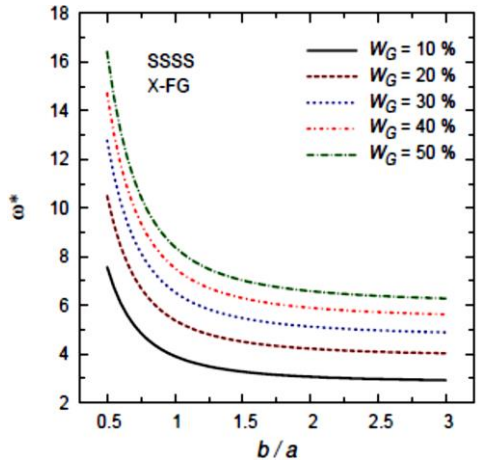

Fig. 5 Frequency ω^* of an SSSS shallow shell versus the aspect ratio b/a for different values of the weight fraction of the graphene W_G $(k=1,\ a/R_1=0.5,\ R_1/R_2=1\ , a/h=10, \overline{K}_1=100,\ \overline{K}_2=50,\ n=r=1)$

plate $(R_1/R_2=0$ and $a/R_1=0)$. For all structures the frequencies decrease as the graded exponent k increases. The frequencies of the FG flat plate are the smallest ones while those for the FG spherical shell are the largest ones.

Table 4 displays the natural frequency ω^* of U-GPLs composite doubly-curved shallow shells for various mode numbers (n,r) and side-to-thickness ratio a/h. It is noted that the natural frequency increases as the mode numbers increases and the ratio a/h decreases. Table 5 reports the fundamental frequencies of FGGPRC doubly-curved shallow shells on elastic foundations. Various types of FG graphene platelet (U-GPLs, X-FG, V-FG and O-FG) are considered in this table. The type U-GPLs gives the highest frequencies while the type O-FG gives the smallest ones. For a fixed value of the Winkler's parameter $\overline{K}_1=100$ the frequency is rabidly increasing as $\overline{K}_2$ increases. While, for a fixed value of the Pasternak's parameter $\overline{K}_1=10$ the frequency is slowly increasing as $\overline{K}_1$ increases. It is to be noted that the frequencies of all types of hyperbolic paraboloidal shells are the smallest comparing with those of both FG spherical and cylindrical shells and also for the FG flat plate.

The influence of different boundary conditions is presented in Table 6. The fundamental frequencies of various types of FGGPRC doubly-curved shallow shells are compared in this table. The fully clamped structures have the greatest frequencies while the fully simply-supported structures have the smallest frequencies.

Now, Figs. 2-8 are presented to illustrate the dimensionless frequency ω^* for various types of FGGPRC doubly-curved shallow shells subjected to different boundary conditions. Fig. 2 shows the influence of power law index k on the dimensionless frequency ω^* of various types of SSSS FG graphene platelet-reinforced composite doubly-curved shallow shells. The frequencies decrease as both a/h and k increase. It is clear that the frequencies are the same when $k=0$, since in this case

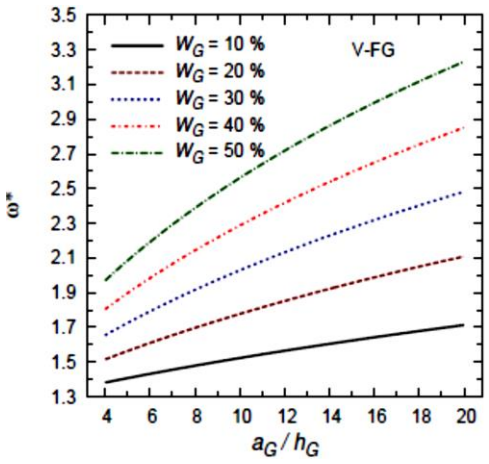

Fig. 6 Frequency ω^* of an SSSS shallow shell versus a_G/h_G for different values of the graphene weight fraction W_G ($k = 1,\ a/R_1 = 0.5,\ R_1/R_2 = 1,\ a/h = 10,\ a = b,\ b_G = a_G,\ \overline{K}_1 = 100,\ \overline{K}_2 = 50,\ n = r = 1$)

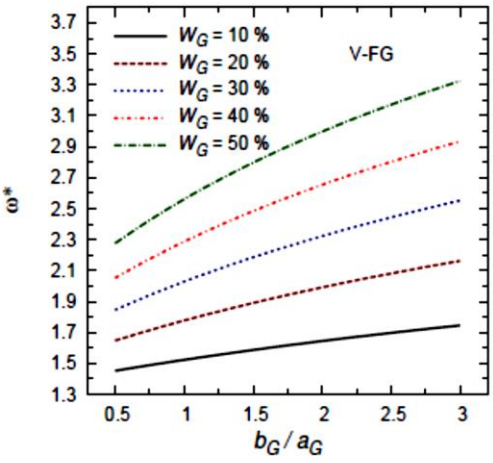

Fig. 7 Frequency ω^* of an SSSS shallow shell versus b_G/a_G for different values of W_G ($k = 1,\ a/R_1 = 0.5,\ R_1/R_2 = 1,\ a/h = 10,\ a = b,\ a_G/h_G = 10,\ \overline{K}_1 = 100,\ \overline{K}_2 = 50,\ n = r = 1$)

there is now difference between all types. Otherwise, the X-FG type gives the highest frequencies while the O-FG type gives the smallest ones.

Fig. 3 shows the variation of the dimensionless frequency ω^* of various types of SSSS and CCCC FGGPRC doubly-curved shallow shells versus the side-to-thickness ratio a/h. As we discussed before the frequencies decrease as a/h increases. Also, the fully clamped structure gives frequencies more than those of the fully simply-supported structure.

Fig. 4 plots the effect of shallowness ratio a/R_1 and aspect ratio b/a on the dimensionless frequency ω^* of an SSSS V-FGGPRC doubly-curved shallow shell. The frequencies increase as a/R_1 increases and b/a decreases. The difference of frequencies may be increase as the aspect ratio b/a increases.

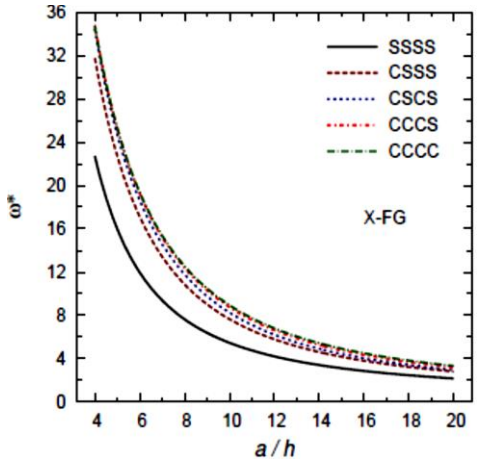

Fig. 8 Frequency ω^* of a shallow shell versus the side-to-thickness ratio a/h for different boundary conditions ($k = 1,\ a/R_1 = 0.5,\ R_1/R_2 = 1,\ b/a = 1.5,\ \overline{K}_1 = 100,\ \overline{K}_2 = 50,\ W_G = 30\%,\ n = r = 1$)

The dimensionless frequency ω^* of an SSSS X-FGGPRC shallow shell versus the aspect ratio b/a for different values of the weight fraction of the graphene W_G is illustrated in Fig. 5. Once again, the frequencies increase as W_G increases and b/a decreases. The difference of frequencies may fixed irrespective the value aspect ratio b/a.

Now, the variation of dimensionless frequency ω^* of an SSSS V-FGGPRC doubly-curved shallow shell for different values of the weight fraction of the graphene W_G is plotted in Fig. 6 versus the a_G/h_G ratio and in Fig. 7 versus the b_G/a_G ratio. As we discussed before, the frequency increases with the increase of the weight fraction of the graphene W_G. Also, the frequency increases with the increase of both a_G/h_G and b_G/a_G ratios.

Finally, Fig. 8 shows the variation of dimensionless frequency ω^* of an X-FGGPRC doubly-curved shallow shell versus the side-to-thickness ratio a/h for different boundary conditions. The following items are discussed before in which the frequency decreases as a/h increases and the fully clamped X-FG structure gives the highest frequencies while the fully simply-supported X-FG structures gives the smallest frequencies.

7. Conclusions

A four-variable shear deformation shell theory has been presented. The free vibration frequencies of functionally graded graphene platelet-reinforced composite doubly-curved shallow shells with different boundary conditions are investigated. The graphene platelets are uniformly distributed in each individual layer and resting on elastic foundation. Two validating examples are investigated for homogeneous and functionally graded structures. The influences of the distribution type of volume fraction, shell curvatures, elastic foundation stiffness and boundary conditions on the vibration of FGGPRC doubly-curved

shells are investigated. For all structures, the fully clamped ones have the largest frequencies while the fully simply-supported ones have the smallest frequencies. Also, the smallest frequencies occur for the homogeneous structures and the frequencies increase with the increase of the power law index. In addition, the increase of the elastic foundation stiffness and graphene weight fraction enhances the strength of the structures and, therefore, leads to an increment in the frequencies. It is also noted that a decrement in the frequencies occurs as the side-to-thickness ratio and aspect ratio increase. While, an increment in the frequencies occurs with the increase of the shallowness ratio and mode numbers.

Acknowledgments

The authors acknowledge the Deanship of Scientific Research at King Faisal University for their support under grant (17122010).

References

Abazid, M.A., Alotebi, M.S. and Sobhy, M. (2018), "A novel shear and normal deformation theory for hygrothermal bending response of FGM sandwich plates on Pasternak elastic foundation", *Struct. Eng. Mech., Int. J.*, **67**(3), 219-232. https://doi.org/10.12989/sem.2018.67.3.219

Arefi, M. (2018), "Nonlocal free vibration analysis of a doubly curved piezoelectric nano shell", *Steel Compos. Struct., Int. J.*, **27**(4), 479-493. https://doi.org/10.12989/scs.2018.27.4.479

Benachour, A., Tahar, H.D., Atmane, H.A., Tounsi, A. and Ahmed, M.S. (2011), "A four variable refined plate theory for free vibrations of functionally graded plates with arbitrary gradient", *Compos. Part B: Eng.*, **42**(6), 1386-1394. https://doi.org/10.1016/j.compositesb.2011.05.032

Bhimaraddi, A. (1991), "Free vibration analysis of doubly curved shallow shells on rectangular planform using three-dimensional elasticity theory", *Int. J. Solids Struct.*, **27**, 897-913. https://doi.org/10.1016/0020-7683(91)90023-9

Bich, D.H., Duc, N.D. and Quan, T.Q. (2014), "Nonlinear vibration of imperfect eccentrically stiffened functionally graded double curved shallow shells resting on elastic foundation using the first order shear deformation theory", *Int. J. Mech. Sci.*, **80**, 16-28. https://doi.org/10.1016/j.ijmecsci.2013.12.009

Bourada, M., Tounsi, A., Houari, M.S.A. and Bedia, E.A.A. (2012), "A new four-variable refined plate theory for thermal buckling analysis of functionally graded sandwich plates", *J. Sandw. Struct. Mater.*, **14**(1), 5-33. https://doi.org/10.1177/1099636211426386

Chandrashekhara, K. (1989), "Free vibrations of anisotropic laminated doubly curved shells", *Comput. Struct.*, **33**(2), 435-440. https://doi.org/10.1016/0045-7949(89)90015-1

Chorfi, S.M. and Houmat, A. (2010), "Nonlinear free vibration of a functionally graded doubly curved shallow shell of elliptical plan-form", *Compos. Struct.*, **92**, 2573-2581. https://doi.org/10.1016/j.compstruct.2010.02.001

De Villoria, R.G. and Miravete, A. (2007), "Mechanical model to evaluate the effect of the dispersion in nanocomposites", *Acta Mater*, **55**(9), 3025-3031. https://doi.org/10.1016/j.actamat.2007.01.007

Duc, N.D. (2013), "Nonlinear dynamic response of imperfect eccentrically stiffened FGM double curved shallow shells on elastic foundation", *Compos. Struct.*, **99**, 88-96. https://doi.org/10.1016/j.compstruct.2012.11.017

Duc, N.D., Seung-Eock, K., Cong, P.H., Anh, N.T. and Khoa, N.D. (2017), "Dynamic response and vibration of composite double curved shallow shells with negative Poisson's ratio in auxetic honeycombs core layer on elastic foundations subjected to blast and damping loads", *Int. J. Mech. Sci.*, **133**, 504-512. https://doi.org/10.1016/j.ijmecsci.2017.09.009

Fadaee, M., Ilkhani, M.R. and Hosseini-Hashemi, S. (2016), "A new generic exact solution for free vibration of functionally graded moderately thick doubly curved shallow shell panel", *J. Vib. Control*, **22**(15), 3355-3367. https://doi.org/10.1177/1077546314551778

Fang, M., Wang, K., Lu, H., Yang, Y. and Nutt, S. (2009), "Covalent polymer functionalization of graphene nanosheets and mechanical properties of composites", *J. Mater. Chem.*, **19**(38), 7098-7105. https://doi.org/10.1039/B908220D

Feng, C., Kitipornchai, S. and Yang, J. (2017), "Nonlinear free vibration of functionally graded polymer composite beams reinforced with graphene nanoplatelets (GPLs)", *Eng. Struct.*, **140**, 110-119. https://doi.org/10.1016/j.engstruct.2017.02.052

Ghavanloo, E. and Fazelzadeh, S.A. (2013), "Free vibration analysis of orthotropic doubly-curved shallow shells based on the gradient elasticity", *Compos. Part B*, **45**, 1448-1457. https://doi.org/10.1016/j.compositesb.2012.09.054

Halpin, J.C. and Kardos, J.L. (1976), "The Halpin-Tsai equations: a review", *Polymer Eng. Sci.*, **16**(5), 344-352. https://doi.org/10.1002/pen.760160512

Hause, T. and Librescu, L. (2007), "Doubly curved anisotropic sandwich panels: Modeling and free vibration", *J. Aircr.*, **44**(4), 1327-1336. https://doi.org/10.2514/1.26990

Hosseini, S.M. and Zhang, C. (2018), "Elastodynamic and wave propagation analysis in a FG graphene platelets-reinforced nanocomposite cylinder using a modified nonlinear micromechanical model", *Steel Compos. Struct., Int. J.*, **27**(3), 255-271. https://doi.org/10.2514/1.26990

Jiang, S., Yang, T., Li, W.L. and Du, J. (2013), "Vibration analysis of doubly curved shallow shells with elastic edge restraints", *J. Vib. Acoust.*, **135**(3), 034502. https://doi.org/10.1115/1.4023146

Karami, B., Janghorban, M., Shahsavari, D. and Tounsi, A. (2018a), "A size-dependent quasi-3D model for wave dispersion analysis of FG nanoplates", *Steel Compos. Struct., Int. J.*, **28**(1), 99-110. https://doi.org/10.12989/scs.2018.28.1.099

Karami, B., Shahsavari, D. and Janghorban, M. (2018b), "A comprehensive analytical study on functionally graded carbon nanotube-reinforced composite plates", *Aerosp. Sci. Technol.*, **82**, 499-512. https://doi.org/10.1016/j.ast.2018.10.001

Karami, B., Shahsavari, D. and Janghorban, M. (2018c), "Wave propagation analysis in functionally graded (FG) nanoplates under in-plane magnetic field based on nonlocal strain gradient theory and four variable refined plate theory", *Mech. Adv. Mater. Struct.*, **25**(12), 1047-1057. https://doi.org/10.1080/15376494.2017.1323143

Karami, B., Shahsavari, D., Janghorban, M., Dimitri, R. and Tornabene, F. (2019), "Wave propagation of porous nanoshells", *Nanomaterials*, **9**(1), 22. https://doi.org/10.3390/nano9010022

Kiani, Y., Akbarzadeh, A.H., Chen, Z.T. and Eslami, M.R. (2012), "Static and dynamic analysis of an FGM doubly curved panel resting on the Pasternak-type elastic foundation", *Compos. Struct.*, **94**(8), 2474-2484. https://doi.org/10.1016/j.compstruct.2012.02.028

Li, L., Li, H., Pang, F., Wang, X., Du, Y. and Li, S. (2017), "The modified Fourier-Ritz approach for the free vibration of functionally graded cylindrical, conical, spherical panels and shells of revolution with general boundary condition", *Math. Probl. Eng.* https://doi.org/10.1155/2017/9183924.

Liew, K.M. and Lim, C.W. (1996), "Vibration of doubly-curved

shallow shells", *Acta. Mech*., **114**(1), 95-119. https://doi.org/10.1007/BF01170398

Liew, K.M. and Lim, C.W. (1997), "Vibration of thick doubly-curved stress free shallow shells of curvilinear planform", *J. Eng. Mech. ASCE*, **123**, 413-421. https://doi.org/10.1061/(ASCE)0733-9399(1997)123:5(413)

Mahdavi, M.H., Jiang, L. and Sun, X. (2012), "Nonlinear free vibration analysis of an embedded double layer graphene sheet in polymer medium", *Int. J. Appl. Mech*., **4**(4), 1250039. https://doi.org/10.1142/S1758825112500391

Matsunaga, H. (2008), "Free vibration and stability of functionally graded shallow shells according to a 2-D higher-order deformation theory", *Compos. Struct*., **84**, 132-146. https://doi.org/10.1016/j.compstruct.2007.07.006

Meziane, M.A.A., Abdelaziz, H.H. and Tounsi, A. (2014), "An efficient and simple refined theory for buckling and free vibration of exponentially graded sandwich plates under various boundary conditions", *J. Sandw. Struct. Mater*., **16**(3), 293-318. https://doi.org/10.1177/1099636214526852

Mochida, Y., Ilanko, S., Duke, M. and Narita, Y. (2012), "Free vibration analysis of doubly curved shallow shells using the superposition-Galerkin method", *J. Sound Vib*., **331**(6), 1413-1425. https://doi.org/10.1016/j.jsv.2011.10.031

Monterrubio, L.E. (2009), "Free vibration of shallow shells using the Rayleigh–Ritz method and penalty parameters", *Arch. Proc. Inst. Mech. Eng. C. J. Mech. Eng. Sci*., **223**(10), 2263-2272. https://doi.org/10.1243/09544062JMES1442

Najafi, F., Shojaeefard, M.H. and Googarchin, H.S. (2017), "Low-velocity impact response of functionally graded doubly curved panels with Winkler–Pasternak elastic foundation: An analytical approach", *Compos. Struct*., **162**, 351-364. https://doi.org/10.1016/j.compstruct.2016.11.094

Nasihatgozar, M., Khalili, S.M.R. and Fard, K.M. (2017), "General equations for free vibrations of thick doubly curved sandwich panels with compressible and incompressible core using higher order shear deformation theory", *Steel Compos. Struct., Int. J*., **24**(2), 151-176. https://doi.org/10.12989/scs.2017.24.2.151

Ni, Z., Bu, H., Zou, M., Yi, H., Bi, K. and Chen, Y. (2010), "Anisotropic mechanical properties of graphene sheets from molecular dynamics", *Physica B*, **405**(5), 1301-1306. https://doi.org/10.1016/j.physb.2009.11.071

Qatu, M.S. and Asadi, E. (2012), "Vibration of doubly curved shallow shells with arbitrary boundaries", *Appl. Acoust*., **73**, 21-27. https://doi.org/10.1016/j.apacoust.2011.06.013

Qatu, M.S. and Leissa, A.W. (1991), "Natural frequencies for cantilevered doubly-curved laminated composite shallow shells", *Compos. Struct*., **17**, 227-255. https://doi.org/10.1016/0263-8223(91)90053-2

Pasternak, P.L. (1954), "On a new method of analysis of an elastic foundation by means of two foundation constants", Gosudarstvennoe Izdatelstvo Literaturi po Stroitelstvu i Arkhitekture, Moscow, 1-56. [In Russian]

Pathak, A.K., Borah, M., Gupta, A., Yokozeki, T. and Dhakate, S.R. (2016), "Improved mechanical properties of carbon fiber/graphene oxide-epoxy hybrid composites", *Compos. Sci. Technol*., **135**, 28-38. https://doi.org/10.1016/j.compscitech.2016.09.007

Pouresmaeeli, S. and Fazelzadeh, S.A. (2016), "Frequency analysis of doubly curved functionally graded carbon nanotube-reinforced composite panels", *Acta Mech*., **227**, 2765-2794. https://doi.org/10.1007/s00707-016-1647-9

Pradyumna, S. and Bandyopadhyay, J.N. (2008), "Free vibration analysis of functionally graded curved panels using a higher-order finite element formulation", *J. Sound Vib*., **318**(1-2), 176-192. https://doi.org/10.1016/j.jsv.2008.03.056

Rafiee, M.A., Rafiee, J., Yu, Z.Z. and Koratkar, N. (2009), "Buckling resistant graphene nanocomposites", *Appl. Phys. Lett*., **95**, 223103. https://doi.org/10.1063/1.3269637

Reddy, J.N. and Liu, C.F. (1976), "A higher-order shear deformation theory of laminated elastic shells", *Int. J. Eng. Sci*., **23**(3), 319-330. https://doi.org/10.1016/0020-7225(85)90051-5

Rezaiee, P.M., Masoodi, A. and Arabi, E. (2018), "Geometrically nonlinear analysis of FG doubly-curved and hyperbolical shells via laminated by new element", *Steel Compos. Struct., Int. J*., **28**(3), 389-401. https://doi.org/10.12989/scs.2018.28.3.389

Sahmani, S. and Aghdam, M.M. (2017), "Nonlinear instability of axially loaded functionally graded multilayer graphene platelet-reinforced nanoshells based on nonlocal strain gradient elasticity theory", *Int. J. Mech. Sci*., **131**, 95-106. https://doi.org/10.1016/j.ijmecsci.2017.06.052

Shahsavari, D., Karami, B., Fahham, H.R. and Li, L. (2018a), "On the shear buckling of porous nanoplates using a new size-dependent quasi-3D shear deformation theory", *Acta Mechanica*, **229**(11), 4549-4573. https://doi.org/10.1007/s00707-018-2247-7

Shahsavari, D., Karami, B. and Li, L. (2018b), "A high-order gradient model for wave propagation analysis of porous FG nanoplates", *Steel Compos. Struct., Int. J*., **29**(1), 53-66. https://doi.org/10.12989/scs.2018.29.1.053

Shahsavari, D., Shahsavari, M., Li, L. and Karami, B. (2018c), "A novel quasi-3D hyperbolic theory for free vibration of FG plates with porosities resting on Winkler/Pasternak/Kerr foundation", *Aerosp. Sci. Technol*., **72**, 134-149. https://doi.org/10.1016/j.ast.2017.11.004

Shen, H.S., Xiang, Y., Lin, F. and Hui, D. (2017), "Buckling and postbuckling of functionally graded graphene-reinforced composite laminated plates in thermal environments", *Compos. Part B*, **119**, 67-78. https://doi.org/10.1016/j.compositesb.2017.03.020

Shimpi, R.P. (2002), "Refined plate theory and its variants", *AIAA J*., **40**, 137-146. https://doi.org/10.2514/2.1622

Singh, A.V. (1999), "Free vibration analysis of deep doubly curved sandwich panels", *Comput. Struct*., **73**(1-5), 385-394. https://doi.org/10.1016/S0045-7949(98)00267-3

Sobhy, M. (2013), "Buckling and free vibration of exponentially graded sandwich plates resting on elastic foundations under various boundary conditions", *Compos. Struct*., **99**, 76-87. https://doi.org/10.1016/j.compstruct.2012.11.018

Sobhy, M. (2014a), "Generalized two-variable plate theory for multi-layered graphene sheets with arbitrary boundary conditions", *Acta Mech*., **225**, 2521-2538. https://doi.org/10.1007/s00707-014-1093-5

Sobhy, M. (2014b), "Natural frequency and buckling of orthotropic nanoplates resting on two-parameter elastic foundations with various boundary conditions", *J. Mech*., **30**, 443-453. https://doi.org/10.1017/jmech.2014.46

Sobhy, M. (2016), "An accurate shear deformation theory for vibration and buckling of FGM sandwich plates in hygrothermal environment", *Int. J. Mech. Sci*., **110**, 62-77. https://doi.org/10.1016/j.ijmecsci.2016.03.003

Sobhy, M. (2018), "Magneto-electro-thermal bending of FG-graphene reinforced polymer doubly-curved shallow shells with piezoelectromagnetic faces", *Compos. Struct*., **203**, 844-860. https://doi.org/10.1016/j.compstruct.2018.07.056

Sobhy, M. (2019), "Levy solution for bending response of FG carbon nanotube reinforced plates under uniform, linear, sinusoidal and exponential distributed loadings", *Eng. Struct*., **182**, 198-212. https://doi.org/10.1016/j.engstruct.2018.12.071

Sobhy, M. and Abazid, M.A. (2019), "Dynamic and instability analyses of FG graphene-reinforced sandwich deep curved nanobeams with viscoelastic core under magnetic field effect", *Compos. Part B*: *Eng*., **174**, 106966.

https://doi.org/10.1016/j.compositesb.2019.106966
Sobhy, M. and Zenkour, A.M. (2018), "Thermal buckling of double-layered graphene system in humid environment", *Mater. Res. Express*, **5**(1), 015028. https://doi.org/10.1088/2053-1591/aaa2ba
Sobhy, M. and Zenkour, A.M. (2019a), "A comprehensive study on the size-dependent hygrothermal analysis of exponentially graded microplates on elastic foundations", *Mech. Adv. Mater. Struct*., 1-15. https://doi.org/10.1080/15376494.2018.1499986
Sobhy, M. and Zenkour, A.M. (2019b), "Wave propagation in magneto-porosity FG bi-layer nanoplates based on a novel quasi-3D refined plate theory", *Waves Random Complex Media*, 1-21. http://doi.org/10.1080/17455030.2019.1634853.
Song, M., Kitipornchai, S. and Yang, J. (2017), "Free and forced vibrations of functionally graded polymer composite plates reinforced with graphene nanoplatelets", *Compos. Struct.*, **159**, 579-588. https://doi.org/10.1016/j.compstruct.2016.09.070
Tan, D.Y. (1998), "Free vibration analysis of shells of revolution", *J. Sound Vib*., **213**(1), 15-33. https://doi.org/10.1006/jsvi.1997.1406
Thai, H.T. and Vo, T.P. (2013), "A new sinusoidal shear deformation theory for bending, buckling, and vibration of functionally graded plates", *Appl. Math. Model*., **37**(5), 3269-3281. https://doi.org/10.1016/j.apm.2012.08.008
Thai, H.T., Nguyen, T.K., Vo, T.P. and Lee, J. (2014), "Analysis of functionally graded sandwich plates using a new first-order shear deformation theory", *Eur. J. Mech-A/Solids*, **45**, 211-225. https://doi.org/10.1016/j.euromechsol.2013.12.008
Tornabene, F. (2011a), "2-D GDQ solution for free vibrations of anisotropic doubly-curved shells and panels of revolution", *Compos. Struct*., **93**(7), 1854-1876. https://doi.org/10.1016/j.compstruct.2011.02.006
Tornabene, F. (2011b), "Free vibrations of anisotropic doubly-curved shells and panels of revolution with a free-form meridian resting on Winkler–Pasternak elastic foundations", *Compos. Struct*., **94**, 186-206. https://doi.org/10.1016/j.compstruct.2011.07.002
Tornabene, F., Fantuzzi, N., Viola, E. and Ferreira, A.J.M. (2013), "Radial basis function method applied to doubly-curved laminated composite shells and panels with a general higher-order equivalent single layer formulation", *Compos. Part B*, **55**(1), 642-659. https://doi.org/10.1016/j.compositesb.2013.07.026
Vlasov, V.Z. and Leontev, N.N. (1966), "Beams, plates and shells on elastic foundations", Israel Program for Scientific Translation, Jeruselam. [Translated from Russian]
Voloshina, E.N. and Dedkov, Y.S. (2014), "General approach to understanding the electronic structure of graphene on metals", *Mater. Res. Express*, **1**(3), 035603. https://doi.org/10.1088/2053-1591/1/3/035603
Wu, H., Kitipornchai, S. and Yang, J. (2017a), "Thermal buckling and postbuckling of functionally graded graphene nanocomposite plates", *Mater. Des*., **132**, 430-441. https://doi.org/10.1016/j.matdes.2017.07.025
Wu, H., Yang, J. and Kitipornchai, S. (2017b), "Dynamic instability of functionally graded multilayer graphene nanocomposite beams in thermal environment", *Compos. Struct*., **162**, 244-254. https://doi.org/10.1016/j.compstruct.2016.12.001
Yang, J., Wu, H. and Kitipornchai, S. (2017a), "Buckling and postbuckling of functionally graded multilayer graphene platelet-reinforced composite beams", *Compos. Struct*., **161**, 111-118. https://doi.org/10.1016/j.compstruct.2016.11.048
Yang, B., Kitipornchai, S., Yang, Y.F. and Yang, J. (2017b), "3D thermo-mechanical bending solution of functionally graded graphene reinforced circular and annular plates", *Appl. Math. Model*., **49**, 69-86. https://doi.org/10.1016/j.apm.2017.04.044
Yavari, F., Rafiee, M., Rafiee, J., Yu, Z.-Z. and Koratkar, N. (2010), "Dramatic increase in fatigue life in hierarchical graphene composites", *ACS Appl. Mater Interfaces*, **2**(10), 2738-2743. https://doi.org/10.1021/am100728r
Zenkour, A.M. and Sobhy, M. (2018), "Nonlocal piezo-hygrothermal analysis for vibration characteristics of a piezoelectric Kelvin–Voigt viscoelastic nanoplate embedded in a viscoelastic medium", *Acta Mech*., **229**(1), 3-19. https://doi.org/10.1007/s00707-017-1920-6
Zenkour, A.M., Allam, M.N.M. and Sobhy, M. (2010a), "Bending analysis of FG viscoelastic sandwich beams with elastic cores resting on Pasternak's elastic foundations", *Acta Mech*., **212**(3-4), 233-252. https://doi.org/10.1007/s00707-009-0252-6
Zenkour, A.M., Allam, M.N.M. and Sobhy, M. (2010b), "Effect of transverse normal and shear deformation on a fiber-reinforced viscoelastic beam resting on two-parameter elastic foundations", *Int. J. Appl. Mech*., **2**(1), 87-115. https://doi.org/10.1142/S1758825110000482
Zhao, X., Zhang, Q., Chen, D. and Lu, P. (2010), "Enhanced mechanical properties of graphenebased poly(vinyl alcohol) composites", *Macromolecules*, **43**(5), 2357-2363. https://doi.org/10.1021/ma902862u

CC